# Effects of wildfire smoke on atmospheric polarization

Joseph A. Shaw*[a], Nathan J. Pust[a], and Elizabeth Forbes[b]
[a]Electrical and Computer Engineering Dept., 610 Cobleigh Hall, Montana State University, Bozeman, MT, USA 59717; [b]Physics Dept., Montana State University, Bozeman, MT, USA 59717

## ABSTRACT

A continuously operating all-sky polarization imager recorded the skylight polarization pattern as conditions transitioned from clear and clean to extremely smoky. This transition included a period when a local wildfire plume filled part of the sky with smoke, creating a highly asymmetric distribution of aerosols. Multiple scattering in the smoke plume strongly reduced the degree of polarization in the smoky region of the sky. Once the smoke plume spread out to cover the entire local sky, the degree of polarization was strongly reduced everywhere. However, this example differed from previously observed smoke events because, even though the usual skylight polarization pattern generally persisted throughout the event, this time the smoke-covered sky exhibited a spatially asymmetric profile along the band of maximum polarization. This pattern of reduced polarization toward the horizon is hypothesized to be a result of an optically thick but physically thin smoke layer. The skylight polarization observations are supplemented with optical depth measurements and aerosol size distribution retrievals from a solar radiometer.

**Keywords:** polarization; skylight; aerosols; smoke; wildfire; biomass burning; all-sky imaging; remote sensing

## 1. INTRODUCTION

Polarization is being explored and used for increasingly diverse applications that include a wide range of military and environmental sensing applications.[1] This also elevates the need for quantitative measurements and models of the effects of scattering by atmospheric gas molecules, aerosols, clouds, and underlying surfaces.[2-7] There have been numerous studies of mitigating the optical and infrared effects of smoke on battlefield conditions,[8-11] and recently there are increasing studies on using polarization for mitigating the adverse effects on imaging by haze and smoke.[12-15] However, there has been a shortage of studies that quantify the effects of smoke on skylight polarization.

Studies of smoke are also useful because aerosols are a major factor in climate and air quality[16-24] and they also significantly alter clouds and precipitation.[25,26] There is a large variation of smoke aerosol properties with fire type (smoldering vs. flaming), the type of vegetation being burned, and distance from the fire,[27,28] so there is a need for smoke studies that can confirm the type, source, and location of the fire. The growing use of polarization for aerosol remote sensing[29-31] also provides motivation to study the smoke and skylight polarization together. There is a particular need to study sky polarization during rapidly changing smoke conditions because the few previous studies of smoke effects on polarization have all been under nominally uniformly smoky skies.[4,32,33]

Smoke is a particularly difficult component of the natural environment to study because it is so highly variable in space and time, yet it has potentially very large effects on optical sensing and imaging. Because of the difficulty of planning for smoke or any other specific set of atmospheric conditions, we developed an all-sky polarization imager that operates outdoors continually.[34] Included in the multi-year data record from this instrument are numerous measurements of sky polarization with overhead smoke layers that have been transported from distant and regional wildfires. However, in August 2012 we obtained measurements before, during, and after a local wildfire that created a smoke plume that rose into the sky almost directly south of our instrument location on the Montana State University campus (45.662ºN, 111.045ºW) in Bozeman, Montana, USA, and spread out so that within approximately twelve hours it had filled the local valley with thick smoke. This unique data set therefore provides an opportunity to observe the effects of a spatially and temporally evolving smoke plume on the skylight polarization pattern.

*jshaw@ece.montana.edu; phone 1 406 994-7261; fax 1 406 994-5958; www.coe.montana.edu/ee/jshaw

Polarization: Measurement, Analysis, and Remote Sensing XI, edited by David B. Chenault, Dennis H. Goldstein,
Proc. of SPIE Vol. 9099, 909907 · © 2014 SPIE · CCC code: 0277-786X/14/$18 · doi: 10.1117/12.2045603

## 2. MEASUREMENT METHODS

### 2.1 All-sky polarization imager

The primary instrument used in this study was the all-sky polarization imager developed at Montana State University.[2-7,32,34] This is a division-of-time imaging polarimeter that uses liquid crystal variable retarders (LCVRs) to tune rapidly through four polarization states rapidly enough to minimize adverse effects of cloud motion. All-sky images are acquired at each of the four polarization states and used in a system-matrix-inversion approach[1] to recover a 4-element Stokes vector at each pixel. This process is repeated at five wavelengths selected with a rotating filter wheel that contains interference filters with half-power bandwidth of 10 nm, centered at 450, 490, 530, 670, and 780 nm for the 2012 version of the instrument. Heaters maintain thermal regulation of the temperature-sensitive LCVRs, and the entire system is calibrated carefully using an integrating sphere and a high-quality rotating polarizer.[2] Figure 1 is a photograph of the all-sky polarization imager enclosed in its all-weather housing, with a fisheye lens looking up at the sky and an automated Sun occulting band that rotates to continually block the Sun from illuminating any portion of the fisheye lens.[34]

Figure 1. Photograph of the Montana State University all-sky polarization imager (right) and solar radiometer (left).

### 2.2 Solar radiometer

Deployed with the custom all-sky polarization imager is a commercial (Cimel) scanning radiometer, which is shown on the left-hand side of the photograph in Figure 1. This instrument enables simultaneous quantification of some key aerosol properties. It operates as part of the NASA-sponsored Aerosol Robotic Network (AERONET)[35] and generates direct measurements of aerosol optical depth (path-integrated extinction) at eight wavelengths from the near ultraviolet to the short-wave infrared (340, 380, 440, 500, 675, 870, 1020, and 1640 nm). Additional properties, such as aerosol size distributions, are retrieved from sky radiance and Sun observations.[36,37,38]

### 2.3 Nephelometer and CAPS PMex Monitor

In a rooftop lab located approximately 0.472 km from the all-sky polarization imager and solar radiometer, we operate several instruments for measuring *in-situ*-sampled aerosol properties. For this study, we used an integrating nephelometer[39] to measure aerosol scattering coefficients at wavelengths of 450 nm, 525 nm, and 635 nm. Aerosol extinction coefficients were measured with a Cavity Attenuation Phase shift Spectroscopy (CAPS) particle extinction monitor (CAPS-PMex)[40] at wavelengths of 450 nm, 530 nm, and 630 nm.

## 3. SMOKE PLUME MEASUREMENTS

### 3.1 Plume evolution over three days

During the afternoon of 28 August 2012, a local wildfire generated a fresh smoke plume in a pine and spruce forest approximately 20 km south of Montana State University in Bozeman, Montana, USA. Prior to the appearance of this plume at approximately 16:30 Mountain Daylight Time (MDT=UTC-6), the sky was clear and quite free of aerosols for this time of year when there is often significant smoke aerosol content arising primarily from distant wildfires. The main plume initially was blown primarily to the northeast, as shown in the photograph of Figure 1, but also occasionally drifted north to our instruments at the university, including some excursions into the direct Sun view of the solar radiometer. At 21:00 MDT, the wind shifted so that it came mostly from the south, bringing the main plume directly over our instruments and quickly filling the valley with smoke. At 03:00 MDT on 29 August, a north wind cleared some of the smoke out of the valley until about midday when calm winds and convection mixed the smoke back into the air over the valley. The smoke thickened dramatically during the afternoon of 29 August so that the setting Sun was barely visible, as shown in the photograph of Figure 3. An unusual west-southwest wind in the hours near midnight on 29 August again reduced the smoke at our measurement site, until again, calmer winds and convection brought smoke back over our site in the late morning on 30 August. A return to more typical easterly evening winds (along with firefighting progress) reduced the smoke and essentially ended this event on 31 August.

Figure 2. Photograph of a wildfire smoke plume rising from the Gallatin National Forest south of Bozeman, Montana at 6:43 PM Mountain Daylight Time (MDT = UTC-6) on 28 August 2012. The left-hand side of this photograph looks east and the right-hand side looks south. The photograph was obtained at a location approximately 2.35 km east-southeast of the all-sky polarization imager. Photograph by J. A. Shaw.

### 3.2 Aerosol optical depth

As a result of the almost completely cloud-free conditions, the solar radiometer operated continually throughout the daylight hours of this event. Its measurements of aerosol optical depth (AOD) at wavelengths of 440 nm, 500 nm, and 675 nm are plotted as a function of time in Figure 4 for 28, 29, and 30 August 2012. This figure shows that the 500-nm AOD was initially at about 0.05, indicating very clean air before the plume appeared. The AOD began to rise slowly after the smoke plume appeared at about 16:30 MDT, and it rose rapidly during the day on 29 August, reaching a peak value of 0.80 at 18:32 MDT on 29 August. Note that these AOD values are measured along the path to the Sun, but reported for a zenith path through the atmosphere. Thus, at 18:32 MDT on 29 August, the zenith atmospheric transmittance at 500 nm was exp(-0.8) = 0.45 (i.e, 45%). The actual atmospheric transmittance would be even lower than

this, however, because of additional attenuation by molecular scattering and absorption, for which the zenith-path transmittance is expected to be on the order of 0.88 according to MODTRAN calculations for our location with no aerosols. Therefore, the total zenith transmittance at 500-nm wavelength would be the product of the aerosol and molecular transmittances, or approximately 0.40 (40%).

As a visual reference, we now briefly consider the atmospheric transmittance at the times of the photographs in Figure 3. The zenith-path transmittance for the 500-nm AOD at 18:08 MDT on 29 August (Figure 3, left) was exp(-0.73) = 0.48, and the actual path transmittance to the Sun (using the AOD multiplied by the secant of the solar zenith angle) was approximately exp[-0.48 × sec(70.2°)] = 0.24 (24%). Similarly, the zenith transmittance for the 500-nm AOD at 19:26 MDT on 29 August (Figure 3, right) was exp(-0.76) = 0.47, while the actual transmittance to the Sun was exp[-0.47× sec(83.7°)] = 0.0138 (1.38%).

Figure 3. Photographs on 29 August 2012: (left) looking southwest at 18:08 MDT with 19.8º solar elevation angle; and (right) looking west at 19:26 MDT with 6.3º solar elevation angle. Photographs by J. A. Shaw.

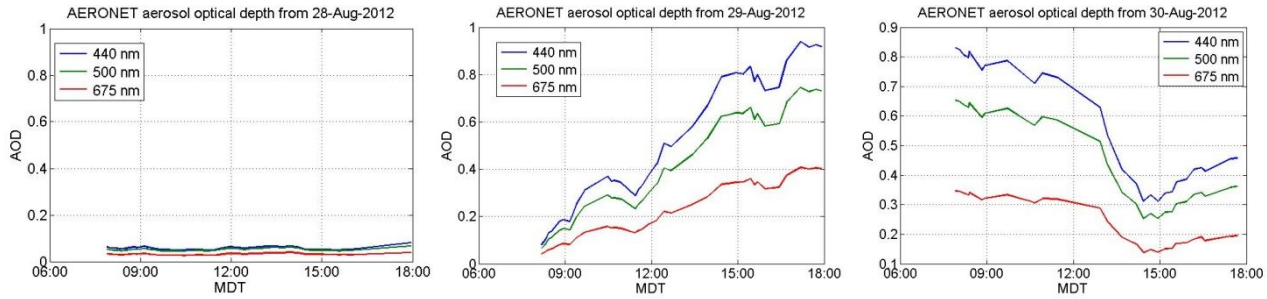


Figure 4. Time-series plots of the aerosol optical depth measured at a wavelength of 500 nm by the solar radiometer.

### 3.3 Aerosol scattering and extinction coefficients

Throughout this event we also had *in-situ* aerosol sampling instruments operating continuously. Figure 5 is a time-series plot of aerosol scattering and extinction coefficients (extinction = scattering + absorption) for aerosols directly sampled at a rooftop lab located approximately 0.472 km north of the all-sky polarization imager. Because these instruments measure aerosols at one point, while the solar radiometer measures the optical effect of aerosols along a path to the Sun, the temporal patterns in Figures 4 and 5 are not expected to correspond exactly; however, there is generally a similar pattern corresponding to the overall evolution of the smoke plume and the smoke layer filling the valley in which our instruments operate. Scattering and extinction coefficients both express the amount of attenuation per unit distance, and both are plotted here in units of $Mm^{-1}$ (i.e., attenuation in a $10^6$ m propagation path). These are standard units in many branches of air quality science, but the numbers can be multiplied by $10^{-3}$ to convert to $km^{-1}$, which are more common units in atmospheric and optical physics. For reference, most populated areas experience typical values of several tens of $Mm^{-1}$, up to perhaps a few hundred $Mm^{-1}$ during pollution episodes. Our location routinely experiences values at or below 10 $Mm^{-1}$, except during summer when the values rise to a few tens of $Mm^{-1}$ because of smoke. The high values

that approach 500 $Mm^{-1}$ on 29 and 30 August correspond to extreme conditions in which the mountains shown in Figure 2 were completely obscured by smoke, as were the distant trees in the right-hand photograph of Figure 3. The previously mentioned difference in measurement geometry for the solar radiometer and *in-situ* aerosol instruments explains how the highest scattering and extinction coefficients could occur at times when the AOD measured by the solar radiometer was lower than its peak value. The highest scattering and extinction coefficients would have occurred when the smoke at the location of our rooftop lab had the highest concentration, but this must have occurred either when the smoke concentration was lower along the path to the Sun or when the physical thickness of the smoke layer was smaller. In other words, this could occur when the smoke was optically thick but physically thin, such that the AOD (the path-integrated extinction) experiences a lower value than at another time when the smoke layer could have been optically thinner but physically thicker.

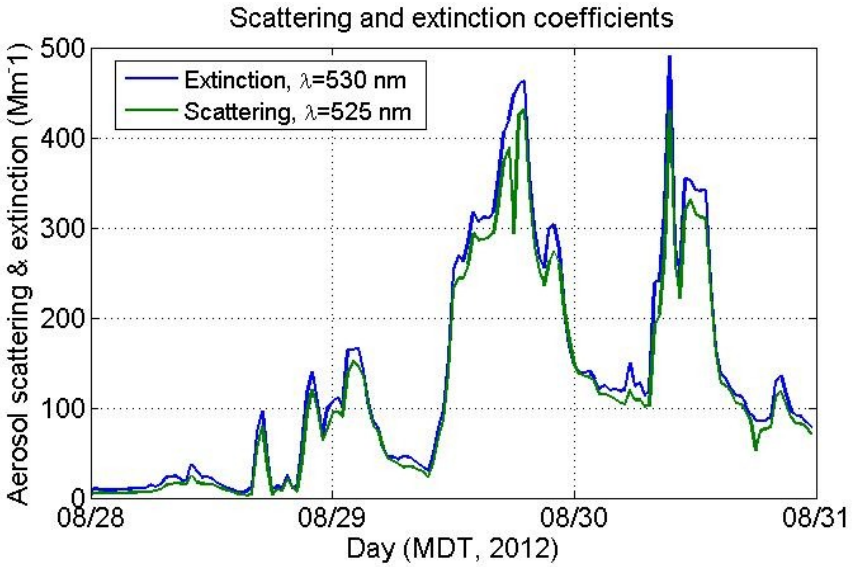


Figure 5. Time-series plots of the 530-nm extinction coefficient measured by a CAPS-PMex monitor and the 525-nm scattering coefficient measured by a 3-wavelength nephelometer.

### 3.4 Skylight polarization measurements

The basic effect of smoke on skylight polarization is to reduce the degree of linear polarization (DoLP) because of increased multiple scattering and to leave the angle of polarization (AoP) unchanged.[1-7,32] In several previous measurements with thick wildfire smoke, the spatial skylight polarization pattern was essentially unchanged, but with a significantly decreased maximum DoLP.[4,32] However, the August 2012 case differed in at least one interesting way: the reduction of the DoLP varied across the "band of maximum polarization" located 90° from the Sun when the smoke was seemingly uniformly spread throughout the overhead sky. This can be seen best by examining Figures 6-8, which show three examples of all-sky polarization images (at a wavelength of 450 nm) on the left, with the corresponding DoLP profile through the "band of maximum polarization" (90° from the Sun) on the right.

The left-hand part of Figure 6 shows an all-sky DoLP image acquired at 16:00 MDT on 28 August 2012, just before the plume appeared to our south. The zenith is nominally at the center of the circular image, and the outside of the circle is the horizon. A small tilt in the system renders these statements not quite correct, but they are generally true. The blue band on the left-hand side of the all-sky image is the metal band that holds the Sun-occulting disk, which appears here at the center of the dark-blue region near the left-hand edge of the all-sky image (i.e, the forward-scattered light from the Sun, as expected, has zero DoLP). The DoLP increases steadily as you move from the Sun at the left-hand edge, toward the right-hand edge of the image, until it reaches a maximum in an arc located 90° from the Sun. With the exception of the small weakly polarized cloud just to the right of the zenith point, this is the pattern predicted by Rayleigh scattering theory for molecular scattering, but with a maximum DoLP that varies with both aerosol content and underlying surface reflectance.[1-7,32] The red line drawn roughly through the center of the "band of maximum polarization" represents a

profile through the DoLP image at a constant 90° scattering angle. This profile is shown as the right-hand portion of Figure 6, plotted as a function of what we refer to as a "dihedral angle" – the angle between a given point on the red arc and the point where the principal plane intersects the band of maximum polarization (this intersection point is where the 90° scattering angle occurs within the principal plane defined by the Sun, the zenith, and the observer). The orientation is such that the left-hand side of the profile corresponds to the top of the all-sky image, which in turn is oriented such that top = south and left = west.

Ignoring the vertical-line artifacts at the edges of the profile plot, the 90° DoLP profile appears quite flat – with the same value of DoLP at all dihedral angles (i.e., at all points located 90° from the Sun, regardless of the zenith angle for those points). The slightly higher DoLP value observed in the southern portion of the sky (left-hand end of the profile and top of the all-sky image) may be a result of differences in the underlying surface reflectance. At this 450-nm wavelength, the conifer-forested mountains to our south appear very dark, while the combination of mature wheat and barley fields and urban areas closer to the polarization imager exhibit a much higher reflectance. From previous studies,[5,7] we know that a less-reflective surface will contribute less upwelling unpolarized light, resulting in a net higher skylight DoLP. Therefore, it is reasonable to assume that the left-hand side of the 90° DoLP profile is higher because that portion of the sky overlies a darker surface than the right-hand side of the profile.

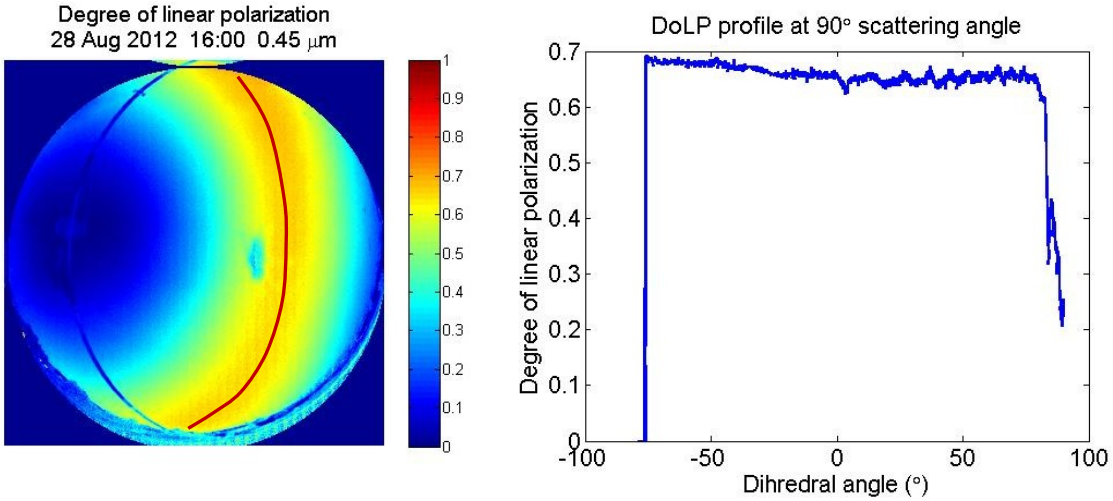


Figure 6. Skylight polarization at 16:00 MDT on 29 August 2012, immediately prior to the appearance of the plume: (left) all-sky image of the degree of linear polarization (DoLP) and (right) DoLP profile along an arc 90º from the Sun (indicated approximately by the red line). The DoLP profile orientation is such that its left-hand side is at the top of the all-sky image, whose orientation is up=south and left=west.

Figure 7 is a similar all-sky DoLP image and 90° DoLP profile, obtained at 1502 MDT on 28 August 2012 as the plume was rising to the south of the polarization imager. In fact, by comparing the all-sky images of Figures 6 and 7, the effect of the plume can be discerned clearly throughout the all-sky image, but especially at its top (south), in Figure 7. The plume's influence can be seen most clearly in the 90° DoLP profile shown on the right-hand side. In this case, the profile is not at all flat, but instead has its lowest point at the left (south) edge closest to the plume, and exhibits seemingly random spatial fluctuations driven by the spatially nonuniform distribution of smoke from the growing plume. The highest point is still at the right-hand (northern) edge of the profile, at the side of the sky situated away from the plume. It is worth noting, however, that even this highest point of the profile is only about 0.5, which is already notably reduced from the value near 0.7 only one hour earlier.

After the plume had filled the valley with relatively uniform smoke, Figure 8 shows an all-sky DoLP image and corresponding 90° DoLP profile from 15:59 MDT on 29 August 2012. In this case, smoke significantly impaired the visibility, such that we could not easily discern the lack of clouds by eye, but yet the usually expected skylight polarization image was still obviously present. However, the 90° DoLP profile exhibits a smooth bowed shape, with the DoLP reaching its maximum somewhat south of the zenith, and falling to smaller values near the southern and northern horizons. With the data we have available, it is impossible to determine the actual uniformity of smoke density, but this bowed DoLP pattern could possibly arise from either: 1) spatial nonuniformities of smoke concentration; or 2) angular variations in "polarimetrically significant" scattering path length.

The latter scenario merits further discussion, as it mixes familiar and unfamiliar ideas into one argument. We begin by considering the familiar increase of scattering path length as solar zenith angle is increased. In other words, as the Sun sets, a stationary observer would experience a decrease of irradiance and a reddening of the spectral distribution. Both effects are caused by an increased atmospheric path length, all of which path contributes to the overall observed irradiance and spectrum. Next, consider the effect of zenith angle on the DoLP of skylight. Whereas there is a very easily discernible brightening of skylight irradiance at the horizon[6], there is normally not a corresponding change of the DoLP. In other words, with the exception of the small tilt that we previously attributed to a spatial variation of underlying surface reflectance, the 90° DoLP profile for the clean- and nearly clear-sky case shown in Figure 6 was essentially flat – certainly with no obvious change near the horizon. This indicates that the observed polarization pattern is dominated by scattering within a relatively short path from the observation point, such that the added path length that would otherwise occur at larger zenith angles is essentially irrelevant for creating or altering the skylight polarization pattern. With this in mind, we can see that a physically thin but optically thick smoke layer could fundamentally change the observed DoLP profile. Specifically, if the physical thickness of the smoke layer is less than the path length from which the primary observed polarization arises, then we would expect to see a reduction of skylight DoLP at larger zenith angles because there is more aerosol scattering along the oblique path through the smoke layer.

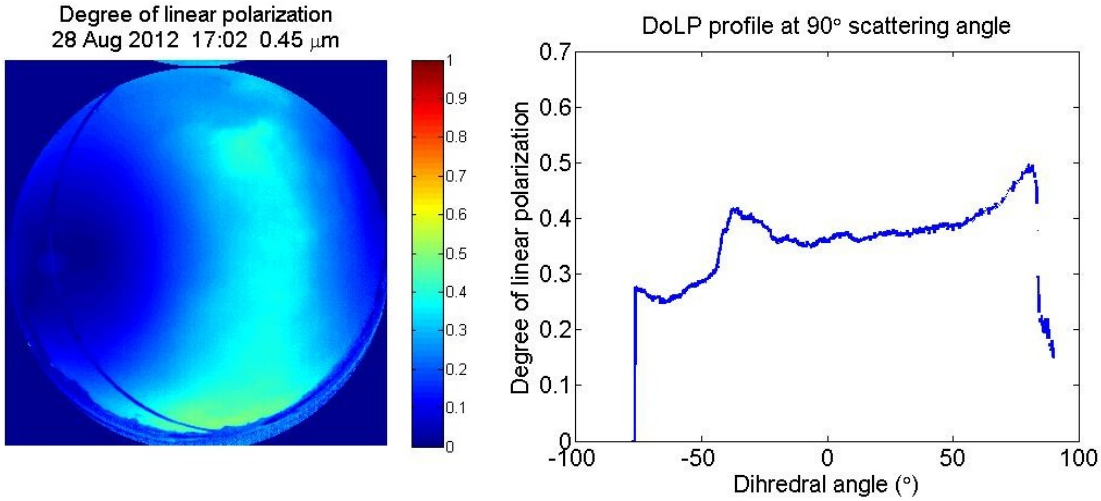


Figure 7. Skylight polarization at 17:02 MDT on 28 August 2012, shortly after the appearance of the plume: (left) all-sky image of the degree of linear polarization (DoLP) and (right) DoLP profile along an arc located 90º from the Sun.

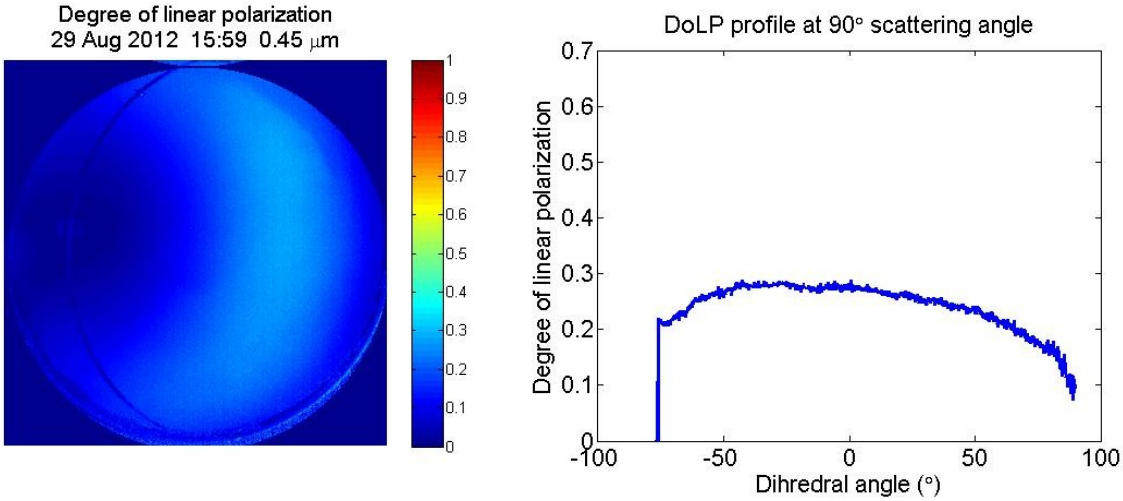


Figure 8. Skylight polarization at 15:59 MDT on 29 August 2012, 24 hours after appearance of the plume, when the valley was filled with smoke: (left) all-sky image of the degree of linear polarization (DoLP) and (right) DoLP profile along an arc located 90º from the Sun

## 4. CONCLUSION

Observations from continuously field-deployed instruments provided a valuable opportunity to study the temporal and spatial variations of skylight polarization during a rapidly evolving wildfire smoke episode in late August 2012. Specifically, we reported measurements of skylight polarization from an all-sky polarization imager, path-integrated aerosol optical depth from a solar radiometer, and aerosol scattering and extinction coefficients from *in-situ* aerosol sampling instruments. The clear-sky polarization pattern that existed before the smoke plume was distorted by increased aerosol scattering in regions with the highest smoke density, but the basic spatial polarization pattern remained otherwise relatively unchanged. The most notable change in the spatial pattern is that with an optically thick but physically thin smoke layer, the DoLP along a profile located 90 from the Sun was reduced near the horizon. This effect does not normally appear in a clear atmosphere, but is hypothesized here to occur when the physical thickness of the smoke layer is less than the atmospheric path length from which the observed polarization pattern primarily arises.

**Acknowledgment**

This material is based on research sponsored by the Air Force Research Laboratory, under agreement number FA9550-10-1-0115. The U.S. Government is authorized to reproduce and distribute reprints for Governmental purposes notwithstanding any copyright notation thereon. The views and conclusions contained herein are those of the authors and should not be interpreted as necessarily representing the official policies or endorsements, either expressed or implied, of the Air Force Research Laboratory or the U.S. Government.

## REFERENCES

[1] Tyo, J. S., Goldstein, D. L., Chenault, D. B. and Shaw, J. A., "Review of passive imaging polarimetry for remote sensing applications," Appl. Opt. 45(22), 5453-5469 (2006).
[2] Pust, N. J. and Shaw, J. A., "Dual-field imaging polarimeter using liquid crystal variable retarders," Appl. Opt. 45, 5470-5478 (2005).
[3] Pust, N. J. and Shaw, J. A., "Digital all-sky polarization imaging of partly cloudy skies," Appl. Opt. 47, H190-H198 (2008).
[4] Pust, N. J. and Shaw, J. A., "Comparison of skylight polarization measurements and MODTRAN-P calculations," J. Appl. Rem. Sens. 5, 053529 (2011).
[5] Dahlberg, A. R., Pust, N. J. and Shaw, J. A., "Effects of surface reflectance on skylight polarization measurements at the Mauna Loa Observatory," Optics Express 19, 16008-16021 (2011).
[6] Pust, N. J., Dahlberg, A. R., Thomas, M. J. and Shaw, J. A., "Comparison of full-sky polarization and radiance observations to radiative transfer simulations which employ AERONET products," Optics Express 19, 18602-18613 (2011).
[7] Pust, N. J. and Shaw, J. A., "Wavelength dependence of the degree of polarization in cloud-free skies: simulations of real environments," Optics Express 20, 15559-15568 (2012).
[8] Butters, B. and Walmsley, R., "Use of a transmissometer model for infrared smoke model validation and assessment of obscuration and detection times," Proc. SPIE 7115, 7115OT (2008).
[9] Chenault, D. B. and Pezzaniti, J. L. "Polarization imaging through scattering media," Proc. SPIE 4133, 124-133 (2000).
[10] Rotman, S. R., Gordon, E. S. and Kowalczyk, M. L., "Modeling human search and target acquisition performance III. Target detection in the presence of obscurants," Opt. Eng. 30(6), 824-829 (1991).
[11] Farmer, W. M., "Analysis of emissivity effects on target detection through smokes/obscurants," Opt. Eng. 30(11) 1701-1708(1991).
[12] Schechner, Y. Y., Narasimhan, S. G. and Nayar, S. K., "Polarization-based vision through haze," Appl. Opt. 42(3), 511-525 (2003).
[13] Namer, E. and Schechner, Y. Y., "Advanced visibility improvement based on polarization filtered images," Proc. SPIE 5888, doi:10.1117/12.617464 (2005).
[14] Miller, D. A. and Dereniak, E. L., "Selective polarization imager for contrast enhancements in remote scattering media," Appl. Opt. 51(18), 4092-4102 (2012).
[15] Mudge, J. and Virgen, M., "Real time polarimetric dehazing," Appl. Opt. 52(9), 1932-1938 (2013).

[16] Kaufman, Y. J., Tanre, D. and Boucher, O., "A satellite view of aerosols in the climate system," Nature 419, 215-223 (2002).
[17] Gyawali, M., Arnott, W. P., Lewis, K., and Moosmüller, H., "In situ aerosol optics in Reno, NV, USA during and after the summer 2008 California wildfires and the influence of absorbing and non-absorbing organic coatings on spectral light absorption," Atmos. Chem. Phys. 9, 8007-8015 (2009).
[18] Spracklen, D. V., Logan, J. A., Mickley, L. J., Park, R. J., Yevich, R., Westerling, A. L. and Jaffe, D. A., "Wildfires drive interannual variability of organic carbon aerosol in the western U.S. in summer," Geophys. Res. Lett. 34, 16, L16816 (2007).
[19] Park, R. J., Jacob, D. J. and Logan, J. A., "Fire and biofuel contributions to annual mean aerosol mass concentrations in the United States," Atmos. Environ. 41, 7389-7400 (2007).
[20] Hodzic, A., Madronich, S., Bohn, B., Massie, S., Menut, L. and Wiedinmyer, C., "Wildfire particulate matter in Europe during summer 2003: meso-scale modeling of smoke emissions, transport and radiative effects," Atmos. Chem. Phys. 7, 4043-4064 (2007).
[21] Hsu, N. C., Tsay,, S.-C., King, M. D. and Herman, J. R., "Deep Blue retrievals of Asian aerosol properties during ACE-Asia," IEEE Trans. Geosci. Rem. Sens. 44, 11, 3180-3195 (2006).
[22] Stohl, A., Andrews, E., Burkhart, J. F., Forster, C., Herber, A., Hoch, S. W., Kowal, D., Lunder, C., Mefford, T., Ogren, J. A., Sharma, S., Spichtinger, N., Stebel, K., Stone, R., Ström, J., Torseth, K., Wehrli, C. and Yttri, K. E., "Pan-Arctic enhancements of light absorbing aerosol concentrations due to North American boreal forest fires during summer 2004," J. Geophys. Res. 111, D22214 (2006).
[23] Al-Saadi, J., Szykman, J., Pierce, R. B., Kittaka, C., Neil, D., Chu, D. A., Remer, L., Gumley, L., Prins, E., Weinstock, L., MacDonald, C., Wayland, R. and Dimmick, F., "Improving national air quality forecasts with satellite aerosol observations," Bull. Amer. Meteor. Soc. 86, 1249-1261 (2005).
[24] Niemi, J. V., Tervahattu, H., Vehkamäki, H., Martikainen, J., Laakso, L., Kulmala, M., Aarnio, P., Koskentalo, T., Sillanpää, M. and Makkonen, U., "Characterization of aerosol particle episodes in Finland caused by wildfires in Eastern Europe," Atmos. Chem. Phys. 5, 2299-2310 (2005).
[25] Sassen, K. and Khvorostyanov, V. I., "Cloud effects from boreal forest fire smoke: evidence for ice nucleation from polarization lidar data and cloud model simulations," Environ. Res. Lett. 3, 025006 (2008).
[26] Andreae, M. O., Rosenfeld, D., Artaxo, P., Costa, A. A., Frank, G. P. Longo, K. M. and Silva-Dias, M. A. F., "Smoking rain clouds over the Amazon, Science 303, 5662, 1337-1342 (2004).
[27] Pratt, K. A., Murphy, S. M., Subramanian, R., DeMott, P. J., Kok, G. L., Campos, T., Rogers, D. C., Prenni, A. J., Heymsfield, A. J., Seinfeld, J. H. and Prather, K. A., "Flight-based chemical characterization of biomass burning aerosols within two prescribed burn smoke plumes," Atmos. Chem. Phys. 11, 12549-12565 (2011).
[28] Eck, T. F., Holben, B. N. Reid, J. S., O'Neill, N. T., Schafer, J. S., Dubovik, O., Smirnov, A., Yamasoe, M. A. and Artaxo, P., "High aerosol optical depth biomass burning events: A comparison of optical properties for different source regions," Geophys. Res. Lett. 30, 20, doi:10.1029/2003GL017861 (2003).
[29] Deuze, J. L., Breon, F. M., Devaux, C., Goloub, P., Herman, M., Lafrance, B., Maignan, F., Marchand, A., Nadal, F., Perry, G. and Tanre, D., "Remote sensing of aerosols over land surfaces from POLDER-ADEOS-1 polarized measurements," J. Geophys. Res. 106, D5, 4913-4926 (2001).
[30] Mischenko, M. I., Cairns, B., Hansen, J. E., Travis, L. D., "Accurate monitoring of terrestrial aerosols and total solar irradiance: Introducing the Glory mission," Bull. Amer. Meteor. Soc. 88, 677-691 (2007).
[31] Diner, D. J., Davis, A., Hancock, B. Gutt, G. and Chipman, R. A., "Dual-photoelastic-modulator-based polarimetric imaging concept for aerosol remote sensing," Appl. Opt. 46, 35, 8428-8445 (2007).
[32] Pust, N. J., "Full sky imaging polarimetry for initial polarized MODTRAN validation," Ph.D. dissertation, Montana State University, http://scholarworks.montana.edu/xmlui/handle/1/2086 (2007).
[33] Hegedus, R., S. Akesson and Horvath, G., "Anomalous celestial polarization caused by forest fire smoke: why do some insects become visually disoriented under smoky skies?" Appl. Opt. 46, 2717-2726 (2007).
[34] Shaw, J. A., Pust, N. J., Staal, B., Johnson, J. and Dahlberg, A. R., "Continuous outdoor operation of an all-sky polarization imager," Proc. SPIE 7672, 76720A, doi:10.1117/12.851374 (2010).
[35] Holben, B. N., Eck, T. F., Slutsker, I., Tanre, D., Buis, J. P., Setzer, A., Vermote, E., Reagan. J. A., Kaufman, Y. J., Nakajima, T., Lavenu, F., Jankowiak, I. and Smirnov, A., "AERONET—A federated instrument network and data archive for aerosol characterization," Rem. Sens. Env. 66(1), 1-16 (1998).
[36] Dubovik, O. and King, M. D., "A flexible inversion algorithm for retrieval of aerosol optical properties from Sun and sky radiance measurements," J. Geophys. Res. 105(D16), 20673-20696, DOI: 10.1029/2000JD900282 (2000).

[37] Smirnov, A. Holben, B. N., Eck, T. F., Dubovik, O. and Slutsker, I., "Cloud-screening and quality control algorithms for the AERONET database," Rem. Sens. Env. 73(3), 337-349 (2000).
[38] Dubovik, O., Smirnov, A., Holben, B. N., King, M. D., Kaufman, Y. J., Eck, T. F. and Slutsker, I., "Accuracy assessments of aerosol optical properties retrieved from Aerosol Robotic Network (AERONET) Sun and sky radiance measurements," J. Geophys. Res. 105(D8), 9791-9806 (2000).
[39] Ecotech, "3-wavelength nephelometer" (5 June 2014). http://www.ecotech.com/particulates/3-wavelength-nephelometer
[40] Massoli, P., Kebabian, P., Onasch, T., Hills, F. and Freedman, A., "Aerosol light extinction measurements by Cavity Attenuated Phase Shift Spectroscopy (CAPS): laboratory validation and field deployment of a compact aerosol extinction monitor," Aerosol Sci. Technol. 44, 428-435 (2010).